

LETTER TO THE EDITOR

# Bar-driven gas redistribution suppresses star formation in spiral galaxies: Evidence from dust lanes in NGC 3351

K. George<sup>1,\*</sup> and S. Subramanian<sup>2,3</sup>

<sup>1</sup> University Observatory, LMU Faculty of Physics, Scheinerstrasse 1, 81679 Munich, Germany

<sup>2</sup> Indian Institute of Astrophysics, Koramangala II Block, Bangalore, India

<sup>3</sup> Leibniz-Institut für Astrophysik Potsdam (AIP), An der Sternwarte 16, D-14482 Potsdam, Germany

May 28, 2026

## ABSTRACT

We present observational evidence, based on high-resolution imaging from HST, ALMA, and AstroSat/UVIT, that the redistribution of gas driven by the bar in the face-on spiral galaxy NGC 3351 results in suppressed star formation in its central regions. Dust and molecular gas coexist in galaxies, allowing dust lanes observed in galaxies to be used to probe the distribution of gas. In the central regions of NGC 3351, covered by the stellar bar, dust lanes are visible in the HST F438W–F814W color map, but surprisingly, these areas lack molecular gas and recent star formation. The inward orientation of the dust lane morphology towards the galaxy’s center suggests that molecular gas may have once been present in this region, but was redistributed to the center due to the stellar bar’s action. The direction of dust lanes, therefore, indicates the past inflows of gas toward the galaxy center, with their morphology consistently oriented inward along the bar. These findings support a scenario where the stellar bar has efficiently channeled molecular gas into the nucleus, building the central reservoir while suppressing star formation along the bar.

**Key words.** galaxies: star formation – galaxies: evolution – galaxies: formation – ultraviolet: galaxies – galaxies: nuclei

## 1. Introduction

The suppression of star formation in regions occupied by a stellar bar, commonly referred to as bar quenching, can contribute to the shutdown of star formation in star-forming spiral galaxies (Man & Belli 2018). Bar quenching operating in the central regions of barred spiral galaxies in the local Universe has been extensively studied (Masters et al. 2010, 2012; Cheung et al. 2013; Gavazzi et al. 2015; James & Percival 2016; Spinoso et al. 2017; Khoperskov et al. 2018; James & Percival 2018; Donohoe-Keyes et al. 2019; George et al. 2019, 2020; Newnham et al. 2020; Percival & James 2020; George & Subramanian 2021; Géron et al. 2021; Scalonì et al. 2024; Renu et al. 2025). However, the physical processes responsible for bar-driven quenching remain poorly understood. This is particularly significant in light of recent James Webb Space Telescope (JWST) observations, which have revealed mature bars at redshifts greater than 1, as well as massive galaxies hosting stellar bars at redshifts around 4, with kinematic evidence indicating ongoing gas redistribution in one such system at a redshift of 2.467 (Kalita et al. 2026; Guo et al. 2025; Géron et al. 2025; Huang et al. 2025). Understanding the role of such bars in quenching star formation at high redshifts and the exact process by which this happens is therefore crucial for constraining the global contribution of different quenching mechanisms in star-forming spiral galaxies.

A key open question is how the bar suppresses star formation. One scenario is that the bar redistributes gas within the central region, effectively removing the fuel for star formation from within the bar’s corotation radius (Combes & Gerin 1985;

Spinoso et al. 2017). A second scenario is that enhanced turbulence, driven by shear and shocks generated by the bar, prevents the gas from collapsing into star-forming clouds (Tubbs 1982; Reynaud & Downes 1998; Verley et al. 2007; Haywood et al. 2016; Khoperskov et al. 2018). Based on a detailed multi-wavelength analysis, George et al. (2019) demonstrated that bar quenching operates in NGC 3351, where a region encompassing the stellar bar is largely devoid of neutral hydrogen, molecular hydrogen, and ongoing star formation. While the absence of gas in the bar region supports a gas redistribution framework, the exact operation of this mechanism remains elusive. Nonetheless, a multiwavelength study of barred galaxies suggests a gradual evolutionary sequence for bar-quenching and outlines a model for this redistribution (George et al. 2020) (see also Scalonì et al. (2024); Renu et al. (2026)).

In this Letter, we explore whether dust lanes can be used as tracers of gas flows in barred galaxies and assess whether their morphology provides insight into the gas redistribution suppressing star formation. Dust grains are formed in the cold interstellar medium from the metals produced by stellar nucleosynthesis and released through stellar winds from evolved stars and supernova explosions that get mixed with the surrounding gas (Draine 2009). Since dust is generally co-spatial with cold gas, molecular hydrogen is often found associated with dust lanes. Along star-forming spiral arms, narrow dust lanes are commonly observed because they are compressed in regions where gas is dense, tracing the dense gas structures. However, in the dynamic action of bar-driven torques, gas and dust can react differently, with the gas reacting quickly and the dust lagging (Marshall et al. 2008; Sánchez-Menguiano et al. 2015). By mapping the distribution and morphology of dust lanes, we can thus trace both the current and past locations of molecular gas within

\* koshyastro@gmail.com

galaxies. We exploit this property to investigate the likely flow of molecular gas in the central region of NGC 3351, particularly within the area influenced by the stellar bar. The dust lanes are identified using an  $F438W - F814W$  color map constructed from high-resolution ( $\sim 0.1''$ ) optical imaging obtained with the Hubble Space Telescope (HST). We also utilize contours from Atacama Large Millimeter/submillimeter Array (ALMA)  $\text{CO}(J = 2-1)$  maps to trace the molecular gas distribution, along with AstroSat/UVIT far-ultraviolet (FUV) imaging to probe recent star formation in the galaxy.

Throughout this letter, we adopt a flat cosmology with  $H_0 = 71$ ,  $\text{km s}^{-1}$ ,  $\text{Mpc}^{-1}$ ,  $\Omega_M = 0.27$ , and  $\Omega_\Lambda = 0.73$  (Komatsu et al. 2011).

## 2. Data and analysis

NGC 3351<sup>1</sup> (also known as Messier 95) is a nearby ( $10 \pm 0.4$  Mpc, Freedman et al. 2001) early-type barred spiral galaxy (Morphology; SBb). The galaxy is nearly face-on galaxy (inclination= $41^\circ$ , position angle= $192^\circ$ ) with a prominent bar. The galaxy has a stellar mass  $\sim 10^{10.4} M_\odot$ , HI mass  $\sim 10^{9.2} M_\odot$ ,  $\text{H}_2$  mass  $\sim 10^9 M_\odot$  and integrated star formation rate  $\sim 0.940 M_\odot/\text{yr}$  (Leroy et al. 2008). The gas phase metallicity ( $12 + \text{Log O/H}$ ) of galaxy is 8.60 (Rémy-Ruyer et al. 2014). We use multiwavelength data of NGC 3351 from the PHANGS survey<sup>2</sup> for the analysis presented here. The PHANGS (Physics at High Angular resolution in Nearby GalaxieS) is a multi-wavelength survey of nearby galaxies carried out with ALMA, Very Large Array (VLA) HI, HST, AstroSat, James Webb Space Telescope (JWST), and the Very Large Telescope (VLT) to understand the interplay of the small-scale physics of gas and star formation with galactic structure and galaxy evolution. The PHANGS-HST survey (Lee et al. 2022) provides high-resolution, multi-band optical imaging from HST; PHANGS-ALMA (Leroy et al. 2021) provides  $\text{CO}(J = 2-1)$  imaging from ALMA; and PHANGS-AstroSat (Hassani et al. 2024) provides FUV imaging from the UVIT instrument onboard AstroSat (Agrawal 2006; Tandon et al. 2017).

We construct an HST  $F438W - F814W$  color map of the galaxy, shown in Fig. 1. The HST  $F438W$  and  $F814W$  images are photometrically calibrated on to the AB system using the zero-point information in the image headers<sup>3</sup>. These HST filter images were chosen to provide a long wavelength baseline, enabling the most effective sampling of the widest wavelength ranges and maximizing the effect of dust extinction. The color map is produced from drizzled imaging data available through PHANGS, with fluxes converted to magnitudes using the zeropoint calibrations. We display only pixels with color values in the range 1.95 to 3.15 mag, chosen to isolate strongly reddened regions associated with dust extinction. We verified that varying this threshold by  $\pm 0.2$  mag does not qualitatively alter the identified dust lane morphology, indicating that our results are robust to the exact choice of color cut. The resulting color map can be considered a proxy for the dust distribution in the galaxy.

<sup>1</sup>  $\alpha(\text{J2000}) = 10:43:57.7$  and  $\delta(\text{J2000}) = +11:42:14$  according to Nasa/IPAC Extragalactic Database (NED).

<sup>2</sup> <http://www.phangs.org/>

<sup>3</sup> <https://www.stsci.edu/hst/instrumentation/acs/data-analysis/zeropoints>

Following George et al. (2019), we use the Spitzer IRAC  $3.6 \mu\text{m}$  image as an extinction-free tracer of the evolved stellar population and can be used to delineate the stellar bar (Meidt et al. 2014). To define the stellar bar, we generate contours from the  $3.6 \mu\text{m}$  image and overlay them (in black), along with contours derived from the ALMA  $\text{CO}(J = 2-1)$  map (in cyan) and the AstroSat/UVIT FUV image (in blue), on the dust map (Fig. 2). We generated contours from the ALMA  $\text{CO}(J = 2-1)$  maps convolved to a lower spatial resolution ( $\sim 15''$ ) than the native-resolution maps ( $\sim 1.5''$ ). Smoothing to a coarser resolution enhances the signal-to-noise ratio of large-scale, faint, and extended structures. Both versions exhibit a similar lack of emission along the bar region, while the native-resolution map further resolves structural features in the central regions and outside the bar. We show the five contour levels for ALMA  $\text{CO}(J = 2-1)$ , corresponding to 1.05, 2.10, 3.15, 4.20, and 5.25  $\text{K km s}^{-1}$ . From the infrared image, we estimate the bar length to be  $\sim 87''$  ( $\sim 4.2 \text{ kpc}$ ). These contours are overlaid on a separate figure, to maintain the clarity of the dust-lane visualization in Fig. 1. Fig. 1 highlights dust lanes in the central region, tracing a spiral-like pattern with varying intensity across the area spanned by the stellar bar. The dust lanes appear to be oriented toward the galaxy center. This is further illustrated in Fig. 2, which shows that the bar region—excluding the central nuclear area—lacks detectable molecular gas and ongoing star formation, yet still exhibits prominent dust lanes (marked by magenta color lines). Prominent dust lanes are distributed along the stellar bar, and they appear particularly concentrated within it. To quantify the spatial relationship between dust, molecular gas, and star formation, we visually compare their distributions and note a systematic offset, with dust lanes extending across regions where  $\text{CO}(J = 2-1)$  and FUV emission are absent along the region covered by the bar. A full pixel-by-pixel correlation analysis is beyond the scope of this Letter but will be explored in future work.

## 3. Discussion

In the local Universe, star-forming barred spiral galaxies are observed to have a depletion of neutral hydrogen and molecular hydrogen within the central sub-kpc and at the ends of the bar, specifically within the bar's corotation radius (Consolandi et al. 2017; George et al. 2020; Newnham et al. 2020). These regions are characterized by no recent star formation and are predominantly composed of evolved stellar populations (James et al. 2009; James & Percival 2015, 2016, 2018; Percival & James 2020; Scaloni et al. 2024; Renu et al. 2025). Simulations reproduce the observational result with regions around the bar showing reduced gas surface density, suppressed star formation, and an older stellar population (Gavazzi et al. 2015; Spinoso et al. 2017; Donohoe-Keyes et al. 2019). These findings suggest that the central regions of spiral galaxies encompassed by the bar can undergo significant star formation suppression.

We examine the phenomenon of star formation suppression in detail, focusing on the stellar bar of NGC 3351, and create a high-resolution optical colour map of the galaxy's central region, which we compare with ALMA  $\text{CO}(J = 2-1)$  and AstroSat/UVIT imaging data.  $\text{CO}(J = 2-1)$  emission is used to trace the bulk molecular gas in galaxies, whereas FUV emission originates from the most recent episodes of star formation. As shown in Fig. 2, despite the presence of dust lanes in the colour map, ALMA  $\text{CO}(J = 2-1)$  observations fail to detect molecular gas down to the  $1\sigma$  mass sensitivity limits of  $\sim$

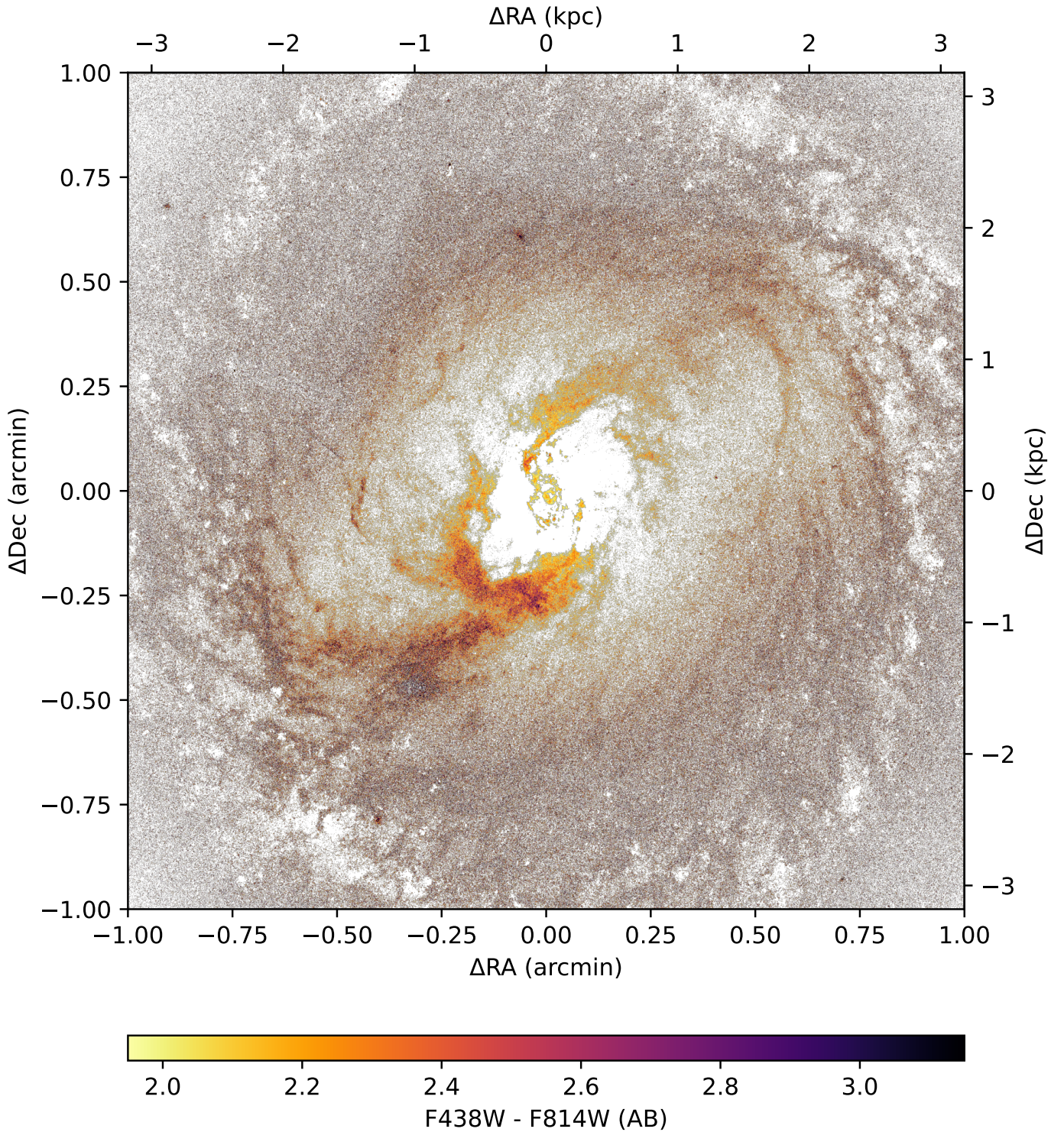


Fig. 1: High-resolution HST  $F438W - F814W$  color map of the central  $\sim 2' \times 2'$  region of NGC 3351. Pixels with values in the range 1.95 to 3.15 in  $F438W - F814W$  are highlighted, corresponding to colors associated with dust lanes. The displayed field corresponds to a physical size of  $\sim 6.36$  kpc on each side.

$2 \times 10^4 M_{\odot}$  at a physical resolution of 100 pc (Leroy et al. 2021). This region is largely devoid of FUV emission, and therefore recent star formation, indicating bar-driven quenching. In contrast, the central region of the bar contains a substantial amount of molecular hydrogen and exhibits ongoing nuclear star formation. Interestingly, dust lanes are detected not only

along the bar but also in regions outside it, yet still within the bar's corotation radius. In these areas,  $CO(J = 2-1)$  emissions remain undetected, while dust structures persist. Since dust typically traces cold gas, the presence of which suggests that gas was once associated with these regions but has since been largely depleted. The dust lanes likely map

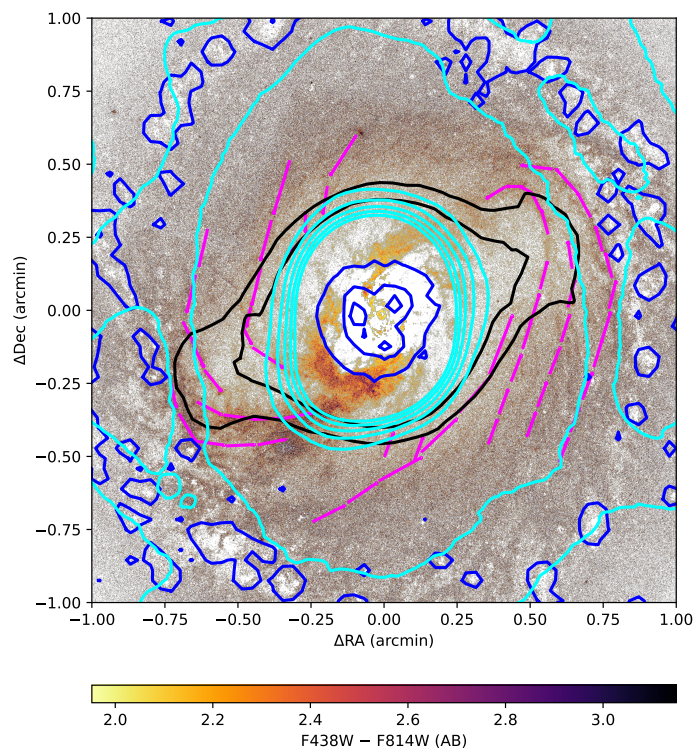


Fig. 2:  $F438W - F814W$  color map of NGC 3351 with the stellar bar (black), Astrosat/UVIT FUV (blue) and ALMA  $\text{CO}(J = 2-1)$  map (cyan) contours overlaid. The location of dust lanes is marked by dashed lines in magenta color.

the pathways of gas redistribution within the bar-influenced central region. Their structural orientations (Fig. 2) support a scenario in which gas flows along the bar as well as through adjacent regions, driving the efficient redistribution of cold gas across the central environment. This provides observational evidence for gas redistribution driven primarily by bar-induced dynamical processes. The most plausible explanation is that gas in NGC 3351 is rapidly transported along the bar, which leaves dust behind, creates a gas-deficient region devoid of fuel for further star formation, and thereby suppresses star formation. While a magnetic-field decoupling scenario can explain spatial offsets between dust and gas along the bar as observed in the Milky Way (Marshall et al. 2008) and NGC 1097 (Beck et al. 2005), the near-complete absence of molecular gas across the wider bar region of NGC 3351 points to a more radical scenario. Here, the prominent dust lanes likely act as structural fossils, tracing the past trajectory of gas that has already been efficiently evacuated and channeled toward the galactic center.

We further investigated the presence of recent star formation along the bar region by examining the  $\text{H}\alpha$  imaging of NGC 3351. The  $\text{H}\alpha$  flux of a galaxy is an indirect tracer of very recent star formation, probing stellar populations younger than  $\sim 10$  Myr, whereas the FUV flux is a more direct tracer of stars with ages up to  $\sim 200$  Myr (Kennicutt & Evans 2012). Figure 14 of Emsellem et al. (2022) presents an RGB image of NGC 3351 in which the  $\text{H}\alpha$  emission (shown in red) is strongly concentrated toward the central regions, with comparatively little emission along the stellar bar. This distribution is consistent with the pattern observed in the AstroSat/FUV flux map shown in Fig. 2, where the FUV emission is likewise predominantly concentrated

toward the central regions of the galaxy. The region where we detect a molecular gas deficiency is also devoid of neutral hydrogen (George et al. 2019), confirming a near-complete lack of total gas content. We estimated the expected bulk molecular hydrogen mass within a  $300 \text{ pc} \times 300 \text{ pc}$  region of the dust lane where ALMA  $\text{CO}(J = 2-1)$  emission was undetected. To isolate the extinction attributable to the dust lane, we subtracted a smooth stellar background from the color map. The resulting  $F438W - F814W$  color excess was then converted into  $A_V$  values using the extinction coefficients from Schlafly & Finkbeiner (2011). We derived a median value of  $A_V = 1 \text{ mag}$  within the probed dust lanes to estimate the gas mass where CO emission was undetected. Using the relation between  $A_V$  and total hydrogen column density ( $N_{\text{H}}$ ), from Bohlin et al. (1978), we derived a bulk molecular hydrogen mass ( $M_{\text{H}_2}$ )  $\sim 1.8 \times 10^6 M_{\odot}$  (assuming  $R_V=3.1$ ). This value is well above the  $1\sigma$  mass sensitivity limit of  $\sim 2 \times 10^4 M_{\odot}$  at a physical resolution of 100 pc reported by Leroy et al. (2021), confirming a lack of molecular hydrogen even under the assumption of a minimal dust content along the bar region. The apparent anti-correlation between dust and  $\text{CO}(J = 2-1)$  emission in this region might alternatively reflect the presence of a diffuse molecular gas phase, which would be more readily detected in the  $\text{CO}(J = 1-0)$  transition due to its lower critical density. However, the  $\text{CO}(J = 1-0)$  map of NGC 3351 presented by Lee et al. (2026) also reveals a distinct deficit of flux along the bar region, consistent with the morphology observed in  $\text{CO}(J = 2-1)$  data. The evidences discussed above indicates that both the dust-lane morphology and the lack of molecular gas and star formation in the bar region are consequences of recent gas funneling toward the galactic center. Because the dust lanes trace the prior path of this gas, these features confirm that bars redistribute the molecular gas, depleting fuel, ultimately triggering star formation quenching within the bar region.

We note that alternative scenarios may also account for the observed star formation activity and molecular gas distribution in the nuclear region of NGC 3351. Leaman et al. (2019) analyzed the gas kinematics and dust lanes at the nuclear regions of NGC 3351 and based on a comparison with stellar feedback models and simulations concluded that the main bar dust lanes are consistent with the expected bar-driven shocks and gas inflow, but the unusual transverse/curved dust lane crossing the bar is not produced by the galaxy's gravitational bar dynamics alone. Instead, they argue it was created by stellar feedback-driven outflow from the circumnuclear star-forming ring. High-resolution imaging reveals two star-forming rings in the central regions, both of which appear to be associated with concentrations of molecular gas, as traced by the  $\text{CO}(J = 2-1)$  maps from the PHANGS survey (Leroy et al. 2021; Ruiz-García et al. 2024) and the  $\text{CO}(J = 3-2)$  maps presented by Sun et al. (2024). It is likely that both the nuclear and outer rings correspond to resonances induced by the stellar bar. Previous studies have identified the corotation radius of the large-scale stellar bar at 2.2 kpc (Ruiz-García et al. 2024; Devereux et al. 1992). The inner molecular ring may correspond to the inner lindblad resonance (ILR) of the large-scale bar, or it could represent the signature of a decoupled or nested molecular-gas bar (Devereux et al. 1992; Shlosman & Heller 2002). In this context, the gas redistribution scenario discussed here may act in addition to these mechanisms, further enhancing the molecular gas concentration in the central region.

Bar-driven gas redistribution may operate efficiently at high redshifts, following the formation of bars in massive galaxies, and could contribute to the shutdown of star formation in their central regions. The evolution of dust lane morphology along the bar over time, observed through snapshots, provides additional insight into this process and can be studied using dust-sensitive colour maps of barred spiral galaxies at different redshifts. Thanks to wide-field optical and near-infrared imaging of galaxies out to redshift  $\sim 1$ , which is becoming available from missions such as *Euclid*, these studies are now within reach (Euclid Collaboration et al. 2025). Furthermore, rapid gas consumption outside the bar, following the suppression of star formation within the bar region, may contribute to the global quenching of star formation in spiral galaxies.

#### 4. Summary

Combining high-resolution HST imaging with ALMA and AstroSat/UVIT observations of NGC 3351, one of the galaxies in the PHANGS survey, we identify areas where gas is likely compressed by creating F438W–F814W color maps and pinpointing dust lanes using a color threshold. We identify a region, spanning from the outer extent of the bar to the vicinity of the galactic center, that shows minimal signs of recent star formation in UVIT FUV imaging and completely lacks molecular gas in ALMA CO( $J = 2-1$ ) maps. However, prominent dust lanes are present along this region and are oriented toward the galaxy center, likely tracing past gas inflow driven by the stellar bar. Recently, gas has been efficiently channeled towards the nucleus, fueling the central molecular gas reservoir and ongoing star formation, while creating a cavity depleted of fuel for further star formation. As a result, star formation is strongly suppressed in the bar region. By applying this dust-lane analysis to a larger sample of barred galaxies, we can investigate systems at different stages of bar-driven gas redistribution and its effect on star formation.

*Acknowledgements.* KG acknowledges the support of DLR through the Euclid@LMU program 50QE2304. SS acknowledges support from the Alexander von Humboldt Foundation. This work makes use of data from the PHANGS (Physics at High Angular resolution in Nearby Galaxies) collaboration, including observations obtained with the NASA/ESA Hubble Space Telescope (PHANGS-HST), the Atacama Large Millimeter/submillimeter Array (PHANGS-ALMA), and AstroSat/UVIT (PHANGS-AstroSat). This paper makes use of the following ALMA data: ADS/JAO.ALMA#2012.1.00650.S, ADS/JAO.ALMA#2015.1.00925.S, ADS/JAO.ALMA#2015.1.00956.S, ADS/JAO.ALMA#2017.1.00886.L, and ADS/JAO.ALMA#2018.1.01651.S. ALMA is a partnership of ESO (representing its member states), NSF (USA), and NINS (Japan), together with NRC (Canada), MOST and ASIAA (Taiwan), and KASI (Republic of Korea), in cooperation with the Republic of Chile. The Joint ALMA Observatory is operated by ESO, AUI/NRAO, and NAOJ. Based on observations made with the NASA/ESA Hubble Space Telescope, obtained from the Mikulski Archive for Space Telescopes (MAST) at the Space Telescope Science Institute (STScI), which is operated by AURA, Inc., under NASA contract NAS 5-26555. This work also uses observations obtained with AstroSat, a mission of the Indian Space Research Organisation (ISRO), archived at the Indian Space Science Data Centre (ISSDC).

#### References

Agrawal, P. C. 2006, *Advances in Space Research*, 38, 12, 2989. doi:10.1016/j.asr.2006.03.038  
 Beck, R., Fletcher, A., Shukurov, A., et al. 2005, *A&A*, 444, 3, 739. doi:10.1051/0004-6361:20053556  
 Bohlin, R. C., Savage, B. D., & Drake, J. F. 1978, *ApJ*, 224, 132. doi:10.1086/156357  
 Cheung, E., Athanassoula, E., Masters, K. L., et al. 2013, *ApJ*, 779, 162  
 Combes, F., & Gerin, M. 1985, *A&A*, 150, 327  
 Consolandi, Guido; Dotti, Massimo; Boselli, Alessandro; Gavazzi, Giuseppe; Gargiulo, Fabio, 2017, *A&A*, 598, 114

Devereux, N. A., Kenney, J. D., & Young, J. S. 1992, *AJ*, 103, 784. doi:10.1086/116100  
 Donohoe-Keyes, C. E., Martig, M., James, P. A., et al. 2019, *MNRAS*, 489, 4, 4992. doi:10.1093/mnras/stz2474  
 Draine, B. T. 2009, *Cosmic Dust - Near and Far*, 414, 453. doi:10.48550/arXiv.0903.1658  
 Emsellem, E., Schinnerer, E., Santoro, F., et al. 2022, *A&A*, 659, A191. doi:10.1051/0004-6361/202141727  
 Freedman, W. L., Madore, B. F., Gibson, B. K., et al. 2001, *ApJ*, 553, 47  
 Gavazzi, G., Consolandi, G., Dotti, M., et al. 2015, *A&A*, 580, A116  
 George, K., Joseph, P., Mondal, C., et al. 2019, *A&A*, 621, L4. doi:10.1051/0004-6361/201834500  
 George, K., Joseph, P., Mondal, C., et al. 2020, *A&A*, 644, A79. doi:10.1051/0004-6361/202038810  
 George, K. & Subramanian, S. 2021, *A&A*, 651, A107. doi:10.1051/0004-6361/202140697  
 Géron, T., Smethurst, R. J., Lintott, C., et al. 2021, *MNRAS*, 507, 3, 4389. doi:10.1093/mnras/stab2064  
 Géron, T., Smethurst, R. J., Dickinson, H., et al. 2025, *ApJ*, 987, 1, 74. doi:10.3847/1538-4357/add7d0  
 Guo, Y., Jogee, S., Wise, E., et al. 2025, *ApJ*, 985, 2, 181. doi:10.3847/1538-4357/ad8a7  
 Hassani, H., Rosolowsky, E., Koch, E. W., et al. 2024, *ApJS*, 271, 1, 2. doi:10.3847/1538-4365/ad152c  
 Haywood, M., Lehnert, M. D., Di Matteo, P., et al. 2016, *A&A*, 589, A66  
 Huang, S., Kawabe, R., Umehata, H., et al. 2025, *Nature*, 641, 8064, 861. doi:10.1038/s41586-025-08914-2  
 Euclid Collaboration, Huertas-Company, M., Walmsley, M., et al. 2025, *arXiv:2503.15311*. doi:10.48550/arXiv.2503.15311  
 James, P. A., Bretherton, C. F., & Knäpen, J. H., 2009, *A&A*, 501, 207  
 James, P. A., & Percival, S. M., 2015, *MNRAS*, 450, 3503  
 James, P. A., & Percival, S. M. 2016, *MNRAS*, 457, 917  
 James, P. A., & Percival, S. M. 2018, *MNRAS*, 474, 3101  
 Kalita, B. S., Ho, L. C., Silverman, J. D., et al. 2026, *ApJ*, 997, 2, 247. doi:10.3847/1538-4357/ae2755  
 Kennicutt, R. C. & Evans, N. J. 2012, *ARA&A*, 50, 531. doi:10.1146/annurev-astro-081811-125610  
 Khoperskov, S., Haywood, M., Di Matteo, P., Lehnert, M. D., & Combes, F. 2018, *A&A*, 609, A60  
 Komatsu E. et al., 2011, *ApJS*, 192, 18  
 Lee, J. C., Whitmore, B. C., Thilker, D. A., et al. 2022, *ApJS*, 258, 1, 10. doi:10.3847/1538-4365/ac1fe5  
 Lee, A. M., Koda, J., Egusa, F., et al. 2026, *ApJ*, 1001, 1, 33. doi:10.3847/1538-4357/ae4d39  
 Leaman, R., Fragkoudi, F., Querejeta, M., et al. 2019, *MNRAS*, 488, 3, 3904. doi:10.1093/mnras/stz1844  
 Leroy, A. K., Walter, F., Brinks, E., et al. 2008, *AJ*, 136, 2782  
 Leroy, A. K., Schinnerer, E., Hughes, A., et al. 2021, *ApJS*, 257, 2, 43. doi:10.3847/1538-4365/ac17f3  
 Man, A. & Belli, S. 2018, *Nature Astronomy*, 2, 695. doi:10.1038/s41550-018-0558-1  
 Marshall, D. J., Fux, R., Robin, A. C., et al. 2008, *A&A*, 477, 2, L21. doi:10.1051/0004-6361:20078967  
 Masters, K. L., Mosleh, M., Romer, A. K., et al. 2010, *MNRAS*, 405, 783  
 Masters, K. L., Nichol, R. C., Haynes, M. P., et al. 2012, *MNRAS*, 424, 2180.  
 Meidt, S. E., Schinnerer, E., van de Ven, G., et al. 2014, *ApJ*, 788, 144  
 Newnham, L., Hess, K. M., Masters, K. L., et al. 2020, *MNRAS*, 492, 4, 4697. doi:10.1093/mnras/staa064  
 Percival, S. M. & James, P. A. 2020, *MNRAS*, 496, 1, 36. doi:10.1093/mnras/staa1369  
 Renu, D., Subramanian, S., Rao, S., et al. 2025, *A&A*, 696, A118. doi:10.1051/0004-6361/202452701  
 Renu, D., Subramanian, S., & George, K. 2026, *arXiv:2604.15208*. doi:10.48550/arXiv.2604.15208  
 Reynaud, D., & Downes, D. 1998, *A&A*, 337, 671  
 Rémy-Ruyer, A., Madden, S. C., Galliano, F., et al. 2014, *A&A*, 563, A31  
 Rodríguez, M. J., Lee, J. C., Indebetouw, R., et al. 2025, *ApJ*, 983, 2, 137. doi:10.3847/1538-4357/adbb69  
 Ruiz-García, M., Querejeta, M., García-Burillo, S., et al. 2024, *A&A*, 691, A351. doi:10.1051/0004-6361/202450935  
 Sánchez-Menguiano, L., Pérez, I., Zurita, A., et al. 2015, *MNRAS*, 450, 3, 2670. doi:10.1093/mnras/stv782  
 Scaloni, L., Rodighiero, G., Enia, A., et al. 2024, *A&A*, 687, A255. doi:10.1051/0004-6361/202449894  
 Schlafly, E. F. & Finkbeiner, D. P. 2011, *ApJ*, 737, 2, 103. doi:10.1088/0004-637X/737/2/103  
 Shlosman, I. & Heller, C. H. 2002, *ApJ*, 565, 2, 921. doi:10.1086/324403  
 Spinoso, D., Bonoli, S., Dotti, M., et al. 2017, *MNRAS*, 465, 3729  
 Sun, J., He, H., Batschkun, K., et al. 2024, *ApJ*, 967, 2, 133. doi:10.3847/1538-4357/ad3de6  
 Tandon, S. N., Subramanian, A., Girish, V., et al. 2017, *AJ*, 154, 3, 128. doi:10.3847/1538-3881/aa8451  
 Tubbs, A. D. 1982, *ApJ*, 255, 458  
 Verley, S., Combes, F., Verdes-Montenegro, L., Bergond, G., & Leon, S. 2007, *A&A*, 474, 43  
 Williams, T. G., Lee, J. C., Larson, K. L., et al. 2024, *ApJS*, 273, 1, 13. doi:10.3847/1538-4365/ad4be5

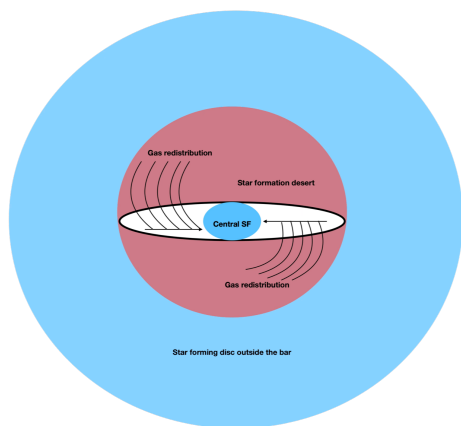


Fig. A.1: Schematic depiction of gas redistribution in NGC 3351 derived from the dust-lane analysis presented in this work. Bar region and disc are not to scale.

### Appendix A: Bar-driven gas redistribution scenario

A schematic illustration of the gas redistribution scenario in NGC 3351 based on the dust analysis presented here is shown in Fig. A.1. The central region, corresponding to the extent of the bar (indicated by the black ellipse), is devoid of star formation (shown in red), while star formation is concentrated in the galaxy center (shown in blue). Gas redistribution occurs throughout the bar region, as indicated by the curved lines, with further transport along the bar toward the center, where star formation is observed. Additional star formation is present in the disk outside the bar region (also shown in blue). The redistribution of gas creates a central concentration, with a kiloparsec-scale region along the bar that is devoid of gas. In the absence of an external supply of gas, the star formation in the centre will deplete the gas completely, and the galaxy will eventually be devoid of star formation in the bar and the central nuclear region.